This article has been accepted for publication in IEEE Transactions on Antennas and Propagation. This is the author's version which has not been fully edited and content may change prior to final publication. Citation information: DOI 10.1109/TAP.2024.3378388

Virtual Polarizer: Coherent Perfect Ultra-wideband Polarization Control Of Chiral Electromagnetic Waves

You-Ran Wu, Rui-Yang Dong, and Hai-Feng Zhang

***Abstract*—In this paper, a novel concept, virtual polarizers (VP), have been proposed through the principles of coherent perfect absorption (CPA) and coherent perfect transparency (CPT) for chiral electromagnetic waves (EWs) to enable polarization control. By interacting and interfering with the signal and control waves, the VP achieves ultra-wideband polarization control for EWs. A structure that implements the VP effect is proposed, realizing polarization control of chiral EWs. The incident polarized waves under consideration have their electric field aligned parallel to the *x*-*y* plane. These EWs can be separated into two polarized waves: transverse electric (TE) waves and transverse magnetic (TM) ones, with components directed along the *x*-axis and *y*-axis, respectively. Transparent propagation is achieved in the 0~2.31 THz band due to CPT, while ultra-wideband coherent perfect polarization conversion is achieved in the 2.72~8.41 THz (102%) band. Through the modulation of InSb layers, VP can realize the perfect control of chirality of phase difference and polarization form of EWs with high polarization conversion efficiency for its arrangement of PT-symmetric structure and implement alteration of the EW propagation. Moreover, the stability of the external parameters is also discussed and considered.**

***Index Terms*— Virtual polarizer; Coherent perfect polarization conversion; Chiral control; Ultra-Wideband modulation.**

I. Introduction

The polarization of the electromagnetic field is a direct result of the vector nature of EWs, and its manipulation holds significant importance in various applications such as optics, and imaging processes [1-3]. The vectorial nature of EW gives rise to different polarization states, which can be linear, circular, or elliptical. These polarization states are defined by the direction and amplitude of the electric field vector as the wave travels across space. The capacity to alter and control polarization provides novel opportunities for applications and technology. Polarization can be controlled by birefringent crystals, dichroic structures, optical gratings, Brewster's phenomenon, metamaterials, and complex materials. Arbitrary output polarization states can be obtained by proper choice of material anisotropy and input polarization [3]. The polarization of the radiated wave in antenna design is typically determined by both the specific application and the characteristics of the propagation environment [4]. Circular polarization waves (CPWs) are favored in satellite communications or navigation systems for their low polarization mismatch losses, increased range, and decreased sensitivity to multipath fading [5-7]. Therefore, effective control of electromagnetic waves (EWs) in small-sized, low-cost structures is of great significance and has a wide range of applications.

A polarizer is a device that selectively filters or modifies the polarization state of EW. Polarizers are designed to transmit EW waves with specific polarization orientations while blocking or attenuating EW waves with different polarizations. In this paper, a novel concept, a virtual polarizer (VP), is proposed. The structure manipulates the polarization of EWs, forming the VP. In fact, the physical polarizers have many limitations compared to the VPs. Firstly, physical polarizers cannot modulate the beam, whereas VPs can arbitrarily manipulate the chiral polarization of the EW. Second, physical polarizers operate at a defined wavelength, which is determined by their sizes, whereas VPs can operate on ultra-wideband. Then, the physical polarizers require a physical composition, whereas VP is a novel idea, that enables manipulating the polarization forms of EWs. Most importantly, the major difference between a VP and a physical polarizer is the requirement for a two-port input. If the input is only at one port, although the structure exists, the effect of polarization is not implemented. The signal EW propagates forward to the VP, and the chiral control EW performs simultaneous control from the backward direction. The structure shall propagate two EWs with completely different polarization states from the incident wave. Since VP is modulated by coherent EW thus achieving the effect of a polarizer which is virtual rather than a physical polarizer. It is described as virtual because it is a new way to manipulate coherent EWs with chirality, ultra-wideband modulation, and convenience, VP has very rich application prospects in polarization coding, sensing, optical switching, logic gates, and other fields [5,8].

Interference, a pervasive wave phenomenon, occurs when two or more coherent waves overlap, resulting in a redistribution of energy across space [9]. This fundamental principle serves as the foundation for the operation of various devices, including antennas, interferometers, and spectrometers. By introducing losses into the system, it gives the system a non-Hermitian nature and consequently a better ability to

This work was supported by the National College Students Innovation and Entrepreneurship Training Program (Grant No.202310293015Z).

You-Ran Wu, and Hai-Feng Zhang with the College of Electronic and Optical Engineering & College of Flexible Electronics, Nanjing University of Posts and Telecommunications, Nanjing, 210023, China. Hai-Feng Zhang is the corresponding author (email:hanlor@163.com or hanlor@njupt.edu.cn).

Rui-Yang Dong with the Bell Honors School & Intensive Courses in Science and Engineering, Nanjing University of Posts and Telecommunications, Nanjing, 210023, China

Authorized licensed use limited to: Nanjing Univ of Post & Telecommunications. Downloaded on April 21,2024 at 10:12:20 UTC from IEEE Xplore. Restrictions apply.
© 2024 IEEE. Personal use is permitted, but republication/redistribution requires IEEE permission. See https://www.ieee.org/publications/rights/index.html for more information.

This article has been accepted for publication in IEEE Transactions on Antennas and Propagation. This is the author's version which has not been fully edited and content may change prior to final publication. Citation information: DOI 10.1109/TAP.2024.3378388

manipulate EWs [10, 11]. When the loss rates are adjusted to achieve critical coupling, the resonator absorbs incoming EW completely without scattering, resulting in a phenomenon known as coherent perfect absorption (CPA). Importantly, this all-optical EW control does not rely on nonlinear phenomena [11]. CPA extends beyond Ohmic absorption and can be applied to other forms of energy conversion, such as storage, polarization conversion (PC), diffraction, and fluorescence [12-17]. Together with coherent perfect transparency (CPT), the system can theoretically achieve arbitrary control of EW propagation characteristics (e.g. polarization, energy, spin angular momentum, etc.) In this study, coherent perfect polarization conversion (CPPC) of EW based on VP is investigated.

Over the past few years, several different types of polarization converters have been documented in the literature. Wang *et al.* [18] introduced a two-dimensional square cavity array structure, which demonstrated a high conversion efficiency in converting incident linear polarization waves (LPWs) into output CPWs. A meandered-line polarizer is described by Young *et al.* [19]. This polarization converter consists of a multilayer structure comprised of meandered metallic strips. The design principle behind this structure is to create an array that exhibits predominantly inductive characteristics for one polarization and capacitive characteristics for the orthogonal polarization. By employing this approach, the meandered-line polarizer achieves efficient PC. Rao *et al.* proposed a layered structure, which enables converting input LPWs into output CPWs, and tunable polarization encoders. Besides, it realized nonlinear bistability to realize manipulation of outgoing EW intensity [5]. Abadi *et al.* introduced a polarization converter based on a miniaturized-element frequency selective surface [4]. However, all the works above are essentially physical polarizers, not virtual ones. They face limitations such as polarizers that cannot be tuned, a defined operating wavelength, and a narrow operating bandwidth. Utilizing the VP, it is possible to achieve ultra-wideband polarization control and chiral arbitrary tuning of coherent EWs using the principles of CPA and CPT.

In this work, a novel innovation point, VP, which is based on a Parity-time (PT)-symmetric structure, is proposed. By controlling the chiral control EWs and signal EWs, the structure is capable of emitting two EWs with completely different polarization states that are chiral to each other. Herein, chirality refers to different polarization modes. Through coherent perfect control, in the low-frequency transparent bands, the VP realizes the CPT of chiral EW, and the two beams of chiral EW do not interact with each other. In CPPC bands, VP realizes the CPA of chiral EW, whose energy is transferred in the form of polarization transition. This will have promising applications in polarization coding. In addition, the structure is calculated to have a remarkably high polarization conversion rate (*PCR*), an exceptionally wide conversion bandwidth, and an incident wave that is compatible with both LPWs and CPWs, which is a very outstanding performance.

II. The Design and Configuration of the VP

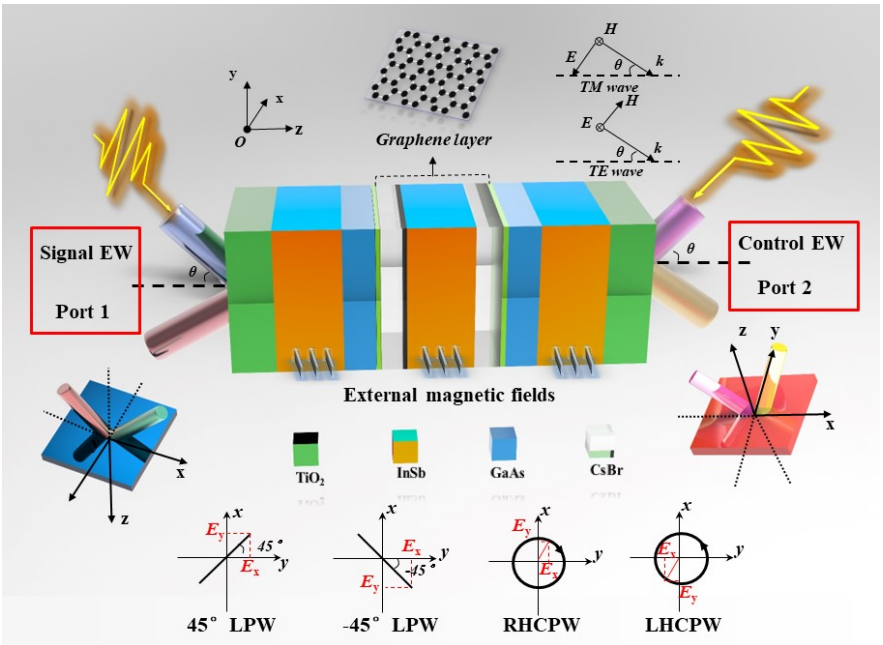

Fig.1. The proposed VP diagram and configuration. The signal waves and the control waves are simultaneously incident obliquely in the forward and backward directions at an angle θ, and the definition of four kinds of polarization states.

The operating principle of the proposed VP is described in Fig.1. The structure illustrated in Fig.1 is described as a VP. As illustrated in Fig.1, +45° LPW denotes the EW, whose direction of the electric field is parallel to the *x*-*y* plane and at an angle of 45° to the *x*-axis, -45° LPW represents the EW, whose electric field direction is parallel to the *x*-*y* plane and at a -45° angle to the *x*-axis. Right-hand circularly polarized wave (RHCPW) refers to an EW whose electric field direction is parallel to the *x*-*y* plane and which is viewed as a clockwise rotating circle in the cross-section of the propagation direction, and left-hand circularly polarized wave (LHCPW) indicates an EW in which the electric field direction is parallel to the *x*-*y*

Authorized licensed use limited to: Nanjing Univ of Post & Telecommunications. Downloaded on April 21,2024 at 10:12:20 UTC from IEEE Xplore. Restrictions apply.
© 2024 IEEE. Personal use is permitted, but republication/redistribution requires IEEE permission. See https://www.ieee.org/publications/rights/index.html for more information.

This article has been accepted for publication in IEEE Transactions on Antennas and Propagation. This is the author's version which has not been fully edited and content may change prior to final publication. Citation information: DOI 10.1109/TAP.2024.3378388

plane and the cross-section in the propagation direction is a circle rotating counterclockwise.

The whole VP is composed of dielectrics titanium dioxide (TiO_2), indium antimonide (InSb), gallium arsenide (GaAs), cesium bromide (CsBr), and graphene layer (GL), and its PT symmetrical structural arrangement belongs to (TiO_2-InSb-GaAs-GL)(GL-CsBr-InSb-CsBr-GL) (GL-GaAs-InSb-TiO_2). For simplicity, the same medium layers have the same thickness. The signal wave incidents forward along the +z-direction, while the control wave incidents backward along the -z-direction at an angle θ. Two counter-propagating waves interfere with each other and CPPC is generated. When the outgoing EW is emitted from port 2 (see Fig.1), the EW that propagates along the +z-direction can be referred to as a forward-propagating, and vice versa as backward propagating EW.

Among them, the refractive indexes of the dielectrics TiO_2, GaAs, and CsBr, are n_{TiO2}=2.25 [10], n_{GaAs}=3.42 [20], and n_{CsBr}=1.15 [21], respectively, and the thicknesses are in sequence d_{TiO2}=9 μm, d_{GaAs}=6.5 μm, d_{CsBr}=5.3 μm, respectively. For clarity, simply the refractive index of the medium is given here, which is a common statement in photonic crystal systems.

In the terahertz (THz） band, the dielectric constant function of InSb has been defined as [5]:

$$\varepsilon_{InSb}=\begin{pmatrix}\varepsilon_x & 0 & i\varepsilon_{xz}\\ 0 & \varepsilon_y & 0\\ -i\varepsilon_{xz} & 0 & \varepsilon_x\end{pmatrix} \tag{1}$$

where

$$\varepsilon_x=\varepsilon_\infty-\varepsilon_\infty\frac{\omega_p^2\left(\omega+i\nu_c\right)}{\omega\left[\left(\omega+i\nu_c\right)^2-\omega_c^2\right]} \tag{1a}$$

$$\varepsilon_y=\varepsilon_\infty-\varepsilon_\infty\frac{\omega_p^2}{\omega\left(\omega+i\nu_c\right)} \tag{1b}$$

$$\varepsilon_{xz}=\varepsilon_\infty\frac{-\omega_p^2\omega_c}{\omega\left[\left(\omega+i\nu_c\right)^2-\omega_c^2\right]} \tag{1c}$$

Herein, ε_∞=15.68 is the high-frequency permittivity and $\omega_p=(e^2N/\varepsilon_0 m^*)^{1/2}$ is the plasma frequency, ν_c=0.00008ω_p is the carrier collision frequency, and the cyclotron frequency is $\omega_c = eB/m^*$, which is proportional to the external magnetic field B [5]. Hereby, the magnetic field strength B is set to 0.3 T, $\omega=2\pi f$ stands for the angle frequency, while f refers to the frequency of EWs. ε_0 means the vacuum dielectric constant and e stands for the electronic power. m denotes the electronic quality and m^*=0.015m. N, for a given temperature T (293 K, typically), is the intrinsic carrier density, which is expressed as [5]:

$$N=5.76\times10^{20}T^{1.5}\exp[-0.26/(2\times8.625\times10^{-5}\times T] \tag{2}$$

When the EWs are incident as the TE and TM modes, the dielectric constants of Insb are [22]:

$$\varepsilon_{InSb(TE)}=\varepsilon_y \tag{3a}$$

$$\varepsilon_{InSb(TM)}=\frac{\varepsilon_x^2-\varepsilon_{xz}^2}{\varepsilon_x} \tag{3b}$$

Considering a graphene layer with a thickness d_G of 0.34 nm, it is possible to realize the modulation of the chemical potential μ_c of GLs by regulating the external voltage.

The surface conductivity σ is associated with the graphene layer and consists of both intraband conductivity σ_{intra}, and interband conductivity σ_{inter} [23-24].

$$\sigma=\frac{ie^2k_BT}{\pi\hbar^2\left(\omega+i/\tau\right)}\left(\frac{\mu_C}{k_BT}+2\ln\left(e^{-\frac{\mu_C}{k_BT}}+1\right)\right)+\frac{ie^2}{4\pi\hbar}\ln\left|\frac{2\mu_C-\hbar\left(\omega+i/\tau\right)}{2\mu_C+\hbar\left(\omega+i/\tau\right)}\right| \tag{4}$$

where $\hbar$, k_B, τ are Planck constant, Boltzmann constant, and relaxation time in turn. Relaxation time τ is set to 0.1 ps [24]. In the absence of any influence from adjacent elements on the electronic band structure of GL, the effective dielectric constant ε_G can be expressed as follows [23]:

$$\varepsilon_G=1+\frac{i\sigma}{\omega\varepsilon_0 d_G} \tag{5}$$

The energy communication between layers is calculated by the transfer matrix method (TMM), which is described in detail in the Supplementary Material Section 1. [22].

$$M_{Total}=\prod_i^{layers}M_i \tag{6}$$

The reflection coefficient R_c and transmission coefficient T_c can be described as follows [8]:

$$R_c=|r|^2 \tag{7}$$

$$T_c=|t|^2 \tag{8}$$

where

$$r=\frac{(m_{11}+m_{12}\eta_{N+1})\eta_0-(m_{21}+m_{22}\eta_{N+1})}{m_{11}\eta_0+m_{12}\eta_0\eta_{N+1}+m_{21}+m_{22}\eta_{N+1}} \tag{9}$$

$$t=\frac{2\eta_0}{m_{11}\eta_0+m_{12}\eta_0\eta_{N+1}+m_{21}+m_{22}\eta_{N+1}} \tag{10}$$

Given the interaction of two counter-propagating EWs, the forward and backward scattering EM fields (O_+ and O_-) can be derived from the incident forward and backward waves (I_+ and I_-), respectively, which can be expressed as follows [8]:

$$\begin{pmatrix}O_+\\ O_-\end{pmatrix}=S\begin{pmatrix}I_+\\ I_-\end{pmatrix}=\begin{pmatrix}t & r\\ r & t\end{pmatrix}\begin{pmatrix}I_+\\ I_-\end{pmatrix}, \tag{11}$$

Assuming that the phase difference between the forward and backward incident waves is Φ, equally, the formula (11) can be expressed as [8]:

$$O_+=t|I_+|+r|I_-|e^{i\Phi}, \tag{11a}$$

$$O_-=r|I_+|+t|I_-|e^{i\Phi}, \tag{11b}$$

where φ_{TM} is the phase of the TM wave, φ_{TE} of the TE wave, and thus the phase difference between the TM and TE waves can be defined as $\Delta\varphi = \varphi_{TM} - \varphi_{TE}$. Hence, the axial ratio (AR) for determining the polarization mode of EW can be calculated as follows [25]:

$$AR=\left(\frac{|O_{TE}|^2+|O_{TM}|^2+\sqrt{a}}{|O_{TE}|^2+|O_{TM}|^2-\sqrt{a}}\right)^{\frac{1}{2}} \tag{12}$$

where

$$a=|O_{TE}|^4+|O_{TM}|^4+2|O_{TE}|^2|O_{TM}|^2\cos(2\Delta\varphi) \tag{12a}$$

Authorized licensed use limited to: Nanjing Univ of Post & Telecommunications. Downloaded on April 21,2024 at 10:12:20 UTC from IEEE Xplore. Restrictions apply.
© 2024 IEEE. Personal use is permitted, but republication/redistribution requires IEEE permission. See https://www.ieee.org/publications/rights/index.html for more information.

This article has been accepted for publication in IEEE Transactions on Antennas and Propagation. This is the author's version which has not been fully edited and content may change prior to final publication. Citation information: DOI 10.1109/TAP.2024.3378388

$$O_{TE(TM),(\pm)} = \left|O_{\pm}\right|^2 \tag{12b}$$

Generally, the polarization of EWs is determined by the AR and phase difference ($\Delta\varphi$) of the EWs. It is universally acknowledged that the AR of CPWs is less than 3dB [5], and the AR of LPWs tends to infinity theoretically.

For the forward propagating output CPWs, $\Delta\varphi$ = -90°±360°n (n = 0, 1, 2⋯) indicates RHCPWs, and $\Delta\varphi$ = 90°±360°n (n = 0, 1, 2⋯) represents LHCPWs. On the contrary, for the backward propagating output CPWs, $\Delta\varphi$ = 90°±360°n (n = 0, 1, 2⋯) stands for RHCPWs, and $\Delta\varphi$ = -90°±360°n (n = 0, 1, 2⋯) means LHCPWs. When $\Delta\varphi$ falls within the range of ±180°±180°n (n = 0, 1, 2⋯), it is classified as an LPW. On the other hand, when $\Delta\varphi$ can take on any value, it is recognized as an elliptically polarized wave (EPW) [5].

In addition, ellipticity χ is also used to specifically quantify the performance of the linear-circular PC [26].

$$\chi = \pm\arctan\left(AR\right) \begin{cases} +, & \varphi_{TE} \geq \varphi_{TM} \\ -, & \varphi_{TE} < \varphi_{TM} \end{cases} \tag{13}$$

In addition, to measure the operating bandwidth of the VP, the relative bandwidth *ffoc* is utilized.

$$ffoc = \frac{2\left(f_H - f_L\right)}{f_H + f_L} \times 100\% \tag{14}$$

where f_L denotes the lower-frequency limit of bands, while f_H denotes the upper-frequency limit of bands.

In this paper, the PC is mainly achieved through the effect of coherence, so the effect of cross-polarization is small and has no impact on the results, and thus the *PCR* can be defined as:

$$PCR = \frac{\left|O_{TE,+}\right|^2 + \left|O_{TM,+}\right|^2 + \left|O_{TE,-}\right|^2 + \left|O_{TM,-}\right|^2}{\left|I_{TE,+}\right|^2 + \left|I_{TM,+}\right|^2 + \left|I_{TE,-}\right|^2 + \left|I_{TM,-}\right|^2} \tag{15}$$

III. Analysis and Discussion

A. The working mechanism of VPs

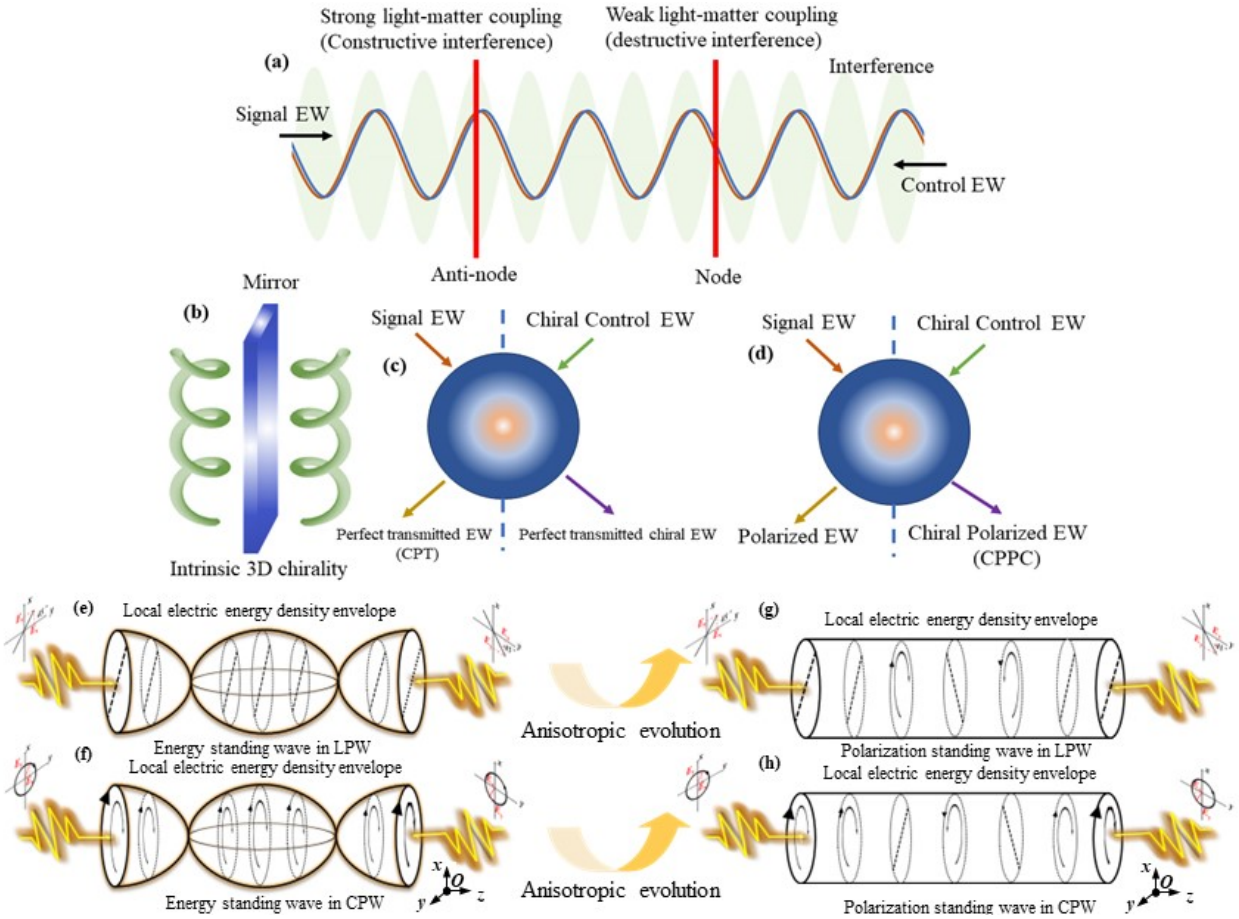

Fig.2. The working mechanism of the VP irradiating under coherent counter-propagating EW. (a) Coherent counter-propagating beams form an interference pattern: constructive interference or destructive interference. EWs have different propagation properties in different polarization directions, creating enhancement or disappearance of electric/magnetic excitation. (b) The chirality in EWs: the polarization state of a wave that cannot be superimposed with its mirror image. Chiral EWs can interact uniquely with chiral materials and structures, leading to various optical phenomena and applications. (c) Chiral CPT, and (d) CPPC in PT-symmetric structures. Local energy standing wave of chiral coherent EW in (e) LPW and (f) CPW when CPPC is realized, and when magnetized InSb has existed in the VP structure as a general anisotropic dielectric, the local electric energy density envelope evolutes, and energy standing wave change to polarization standing wave as in (g) LPW and (h) CPW shows.

Authorized licensed use limited to: Nanjing Univ of Post & Telecommunications. Downloaded on April 21,2024 at 10:12:20 UTC from IEEE Xplore. Restrictions apply.
© 2024 IEEE. Personal use is permitted, but republication/redistribution requires IEEE permission. See https://www.ieee.org/publications/rights/index.html for more information.

This article has been accepted for publication in IEEE Transactions on Antennas and Propagation. This is the author's version which has not been fully edited and content may change prior to final publication. Citation information: DOI 10.1109/TAP.2024.3378388

Fig.2 (a) presents the interference of two equal intensities of coherent waves. The manipulation of the layered photonic structure allows the nature of EW propagation inside the structure to be controlled, and the two coherent EWs produce a strong EW-matter coupling when the outgoing interface is located at the anti-node. In this case, the VP generates constructive interference, leading to enhanced electrical/magnetic excitation of the material. On the contrary, the two coherent beams produced a weak EW-matter coupling at the wave node, and the effect of CPPC is not obvious. At this point, the two coherent EWs produced destructive interference, which led to the weakening of the electric/magnetic excitation. The CPT effect is evident from the characterization of the propagation. Linear dichroism and linear birefringence are anisotropic optical properties that lead to phase delays and differential transmission of ordinary and extraordinary linear characteristic polarizations of anisotropic materials. The utilization of these features helps in the manipulation of the polarization of EW. Hereby, InSb, as an anisotropic material, has different properties in the ordinary and extraordinary polarization performance, which enables better manipulation of the phase and transmission properties of EWs.

Chirality is a fundamental concept in various scientific fields, including chemistry, biology, and physics. As shown in Fig.2 (b), it describes the properties of an object or system that cannot be superimposed on its mirror image. In the field of electromagnetism, chirality refers to the state of propagation of EWs, primarily the state of polarization of the wave. Polarization describes the direction of the electric field vector as the wave propagates through space. CPWs consist of an electric field vector that rotates in a circular pattern as the wave propagates.

In a system where gain/loss exists, CPT [27] and CPA in different frequency bands can be realized for two beams of chiral coherent EW by modulating the effect of the anisotropic medium in different frequency bands using the TMM. CPA is not only limited to ohmic absorption but can also be expanded to other forms of energy conversion, including storage, PC, diffraction, and fluorescence [12-17]. The CPA phenomenon has been explored in a variety of environments and offers applications for a wide range of EW control and management [11]. The VP proposed in this paper can realize CPA and CPT in different frequency bands to control EWs. As demonstrated in Fig.2(c), the manifestation of the CPT [27] phenomenon is that two coherent EWs pass through the VP and obtain a chiral EW with the same electromagnetic properties as before. As indicated in Fig.2(d), CPPC manifests itself when two mutually chiral signal EWs and control EWs are incident, and the VP can emit two EWs with completely different mutually chiral polarization states.

When a chiral coherently propagating EW is incident, as Figs.2(e) and (f) exhibit, the local electric and magnetic field strengths vary along the axes, and the total energy remains unchanged because the nodes of the electric field correspond to the antinodes of the magnetic field, and the nodes of the magnetic field correspond to the antinodes of the electric field, and thus the local electric field polarization form of the energy standing wave is maintained unchanged. A standing wave formed by a chiral LPW maintains the same line polarization at all points along the wave in Fig.2(e), and the same is applicable to CPW. When the anisotropic dielectric InSb is present in the structure, the local energy density envelope changes accordingly. Polarization standing wave occurs as Figs.2 (g) and (h) exhibit. Differently, the locally polarized states oscillate along the wave axis while the electric, magnetic, and total energy densities remain unchanged, and various polarization states are exhibited at different positions of the wave axis. In the transparent band, the chiral coherent EW forms an energy standing wave, and in the high-frequency CPPC band, the polarization standing wave is formed due to the modulation of the anisotropic dielectric, which causes the local polarization state to change. Thus, due to the energy standing wave, the VP forms a transparent band so that the polarization state of the emitted wave does not change, and the chiral polarization control of the emitted wave is formed because of the CPPC band formed by the polarization standing wave.

B. The parameters for coherent polarization control

As already described in section II regarding the initial parameters of the VP, the phase difference between the TM and TE waves can be defined as $\Delta\varphi = \varphi_{TM} - \varphi_{TE}$.

AR is a measurement parameter used to quantify polarization in EWs. It provides information about the ellipticity or circularity of the polarization state of a wave. The AR is defined as the ratio of the major axis to the minor axis of the polarization ellipse (PE). It provides the ability to visually assess the polarization quality and characteristics of EWs, which helps in the optimization and performance evaluation of polarization systems. Ideally, a CPW has an AR of 0 dB, and it is generally accepted that any EW with an AR of less than 3 dB can be considered a CPW [5].

As shown in Fig.3, the polarized forms of the four kinds of signal EWs are investigated, and the polarization properties of their resulting forward and backward EWs output at the two ports are studied.

When the incident signal EW is +45° LPWs, as shown in Fig.3(a), the VP can emit CPWs in the range of 2.735~8.39 THz. Based on the analysis, the relative bandwidth *ffoc* of the entire VP capable of achieving the +45° linear-circle polarization transition for chiral output is 102.2%, which can be considered as the polarization transition region of the ultra-wideband.

According to the above structure, the EW emitted by port 1 (see Fig.1) is backward-propagating, while the EW emitted by port 2 (see Fig.1) is forward-propagating, and therefore, the EW propagating in the forward direction is LHCPW, while the EW propagating in the backward direction is RHCPW. Similarly, Fig.3(b) shows the properties of the outgoing EW at two ports of the VP when the -45° LPW is incident. According to the simulation structure, it can be obtained that when the -45° LPW is incident, the VP can output the backward-propagating LHCPW at port 1, while outputting the forward-propagating RHCPW at port 2.

When the signal EW is incident as a CPW and the control EW is incident at the same time as its chiral symmetry, the

Authorized licensed use limited to: Nanjing Univ of Post & Telecommunications. Downloaded on April 21,2024 at 10:12:20 UTC from IEEE Xplore. Restrictions apply.
© 2024 IEEE. Personal use is permitted, but republication/redistribution requires IEEE permission. See https://www.ieee.org/publications/rights/index.html for more information.

This article has been accepted for publication in IEEE Transactions on Antennas and Propagation. This is the author's version which has not been fully edited and content may change prior to final publication. Citation information: DOI 10.1109/TAP.2024.3378388

properties of the EW output from the VP are illustrated in Figs.3(c) and (d). When the structure of an LHCPW incident on the VP, the VP can output the backward-propagating -45° LPW at port 1, while outputting the forward-propagating 45° LPW at port 2. Whereas, when RHCPWs incident on VP, the VP is capable of outputting the backward-propagating 45° LPW at port 1, while outputting the forward-propagating -45° LPW at port 2.

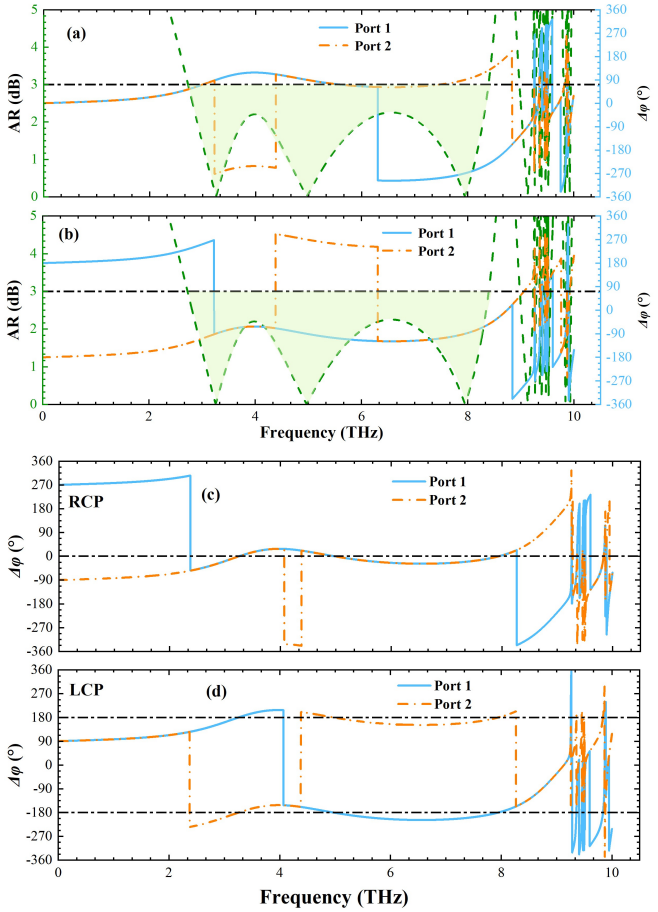

Fig.3. The EW characteristics of the two port outputs of the VP are investigated. They are categorized into four main cases as follows: The input signal EW is (a)+45° linear polarization, (b) -45° linear polarization, (c) right-hand circular polarization, and (d) left-hand circular polarization.

TABLE I.
THE POLARIZATION RELATIONSHIP BETWEEN THE SIGNAL LIGHT AND CHIRAL OUTPUT EWS.

Signal EW	Control EW	Port 1 (-z propagating)	Port 2 (+z propagating)
45° LPW	-45° LPW	LHCPW	RHCPW
-45° LPW	45° LPW	RHCPW	LHCPW
LHCPW	RHCPW	-45° LPW	45° LPW
RHCPW	LHCPW	45° LPW	-45° LPW

Overall, the polarization relationship between the chiral output EW and the signal EW can be clearly interpreted in Table I. First, as indicated in Fig.4, the operating properties of the VP when the signal wave is incident with a 45° LPW are investigated.

Fig.4(a) illustrates the relationship between the phase difference between the TM and TE waves when the +45° LPW is incident through the VP. Fig.4(b) demonstrates the trend of the AR with frequency, bounded by 3 dB, and the VP is capable of achieving ultra-wideband CPPC from 2.735 to 8.39 THz, with mutually chiral CPW output. In this operating bandwidth, there are three perfectly matching points with an AR of exactly 0 dB. At these three frequency points, the phase difference between TM and TE waves is exactly 90 ° apart, and the VP can output a perfect CPW. As shown in Fig.4(c), the output EW intensity of the VP operating in different modes illustrates that in the operating frequency band, the VP has almost no loss of the intensity of the EWs.

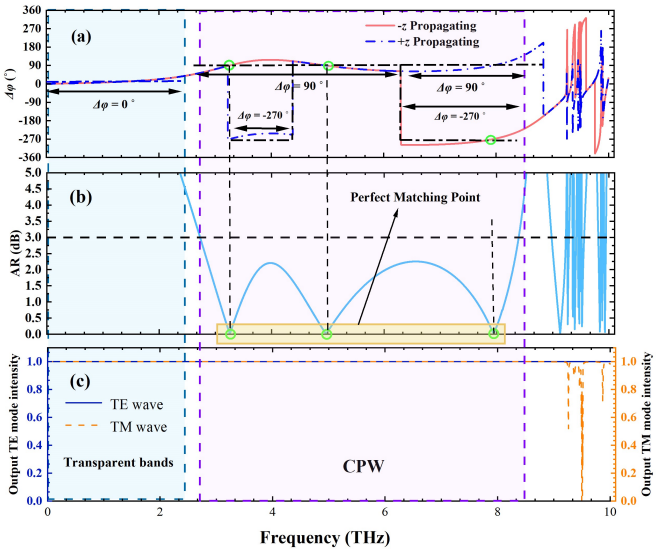

Fig.4. Output intensities and polarization characteristics of VP in 0~10 THz (a) The variation of phase difference $\Delta\varphi$ with frequency, (b) Variation of the AR with frequency, and (c) Output characteristics of VP in the operating frequency band.

At 0~2.2 THz, the VP exhibits CPT-based transparent bands (CTBs) where the signal EWs (45° LPWs) and its reciprocally chiral phase-propagating LPWs are mutually constructive interference. During this process, the EW intensity and polarization states of the two beams of EW hardly change. Therefore, it can be viewed as a CTB. Meanwhile, at 2.735~8.39 THz, the manipulation of EWs by VP reveals the role of ultra-wideband CPPC. In this band, the interaction of the signal EWs (45° LPWs) and the linear-polarized control EW with its reciprocal chirality results in two reciprocally chiral CPWs with different propagation directions.

Take the case of a forward propagating output EM wave at port 2, as illustrated in Fig.5(a), the ellipticity χ of the PE is calculated, which helps us to measure the performance of the polarization transition.

When the ellipticity χ is around 45°, it can be recognized as RHCPW, when the ellipticity χ is close to 0 it can be regarded as LPW, and when the ellipticity χ is close to -45° it can be regarded as LHCPW. The stimulated PEs for 1.8 THz, 3.24 THz, and 8.74 THz are shown in Figs.5(b)~(d), respectively. Remarkably, a perfect right-handed polarization circle was obtained out at 3.24 THz. In addition, at other frequencies, the PE is symmetric about the line E_x=E_y, since the effect of cross-polarization is neglected. At 8.74 THz, the PE becomes a line, at which point the ellipticity χ is 0.

Authorized licensed use limited to: Nanjing Univ of Post & Telecommunications. Downloaded on April 21,2024 at 10:12:20 UTC from IEEE Xplore. Restrictions apply.
© 2024 IEEE. Personal use is permitted, but republication/redistribution requires IEEE permission. See https://www.ieee.org/publications/rights/index.html for more information.

This article has been accepted for publication in IEEE Transactions on Antennas and Propagation. This is the author's version which has not been fully edited and content may change prior to final publication. Citation information: DOI 10.1109/TAP.2024.3378388

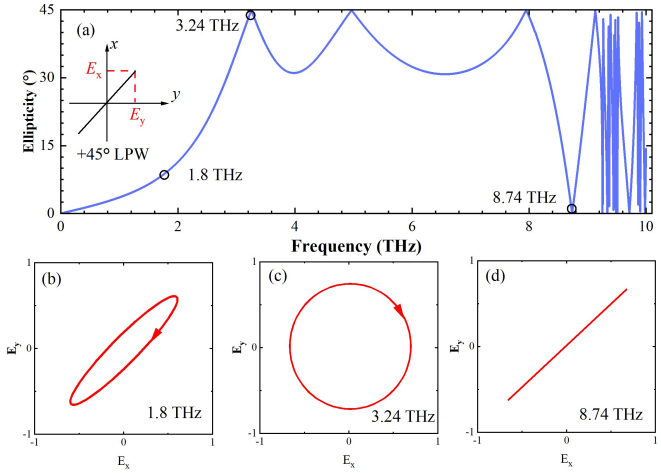

Fig.5. (a) The ellipticity χ of the PE at different operating frequencies, and the PE at three frequencies when the signal EW is +45° LPW (b) 1.8 THz, (c) 3.24 THz, and (d) 8.74 THz.

Next, the case where the signal EW is incident with a -45° linear polarization and coherently incident with its reciprocal chiral LPW is discussed.

Fig.6(a) illustrates the relationship between the phase difference of the TM and TE waves when the -45°LPW is incident on the VP. The trend of the AR with frequency is investigated in Fig.6(b), confined within a 3 dB boundary. Equally, the VP demonstrates its impressive capability of achieving ultra-wideband CPPC from 2.735 to 8.39 THz, generating mutually chiral CPW as output. Within this operating bandwidth, three perfectly matching points (3.24 THz, 4.986 THz, and 7.936 THz) are found with an AR of exactly 0 dB. At these frequencies, the phase difference between the TM and TE waves is precisely 90°, resulting in the ability of the VP to produce a perfect CPW. Fig.6(c) presents the output EW intensity for the VP operating in different modes. Notably, within the operating frequency range, the VP exhibits minimal loss in the intensity of the EWs it produces.

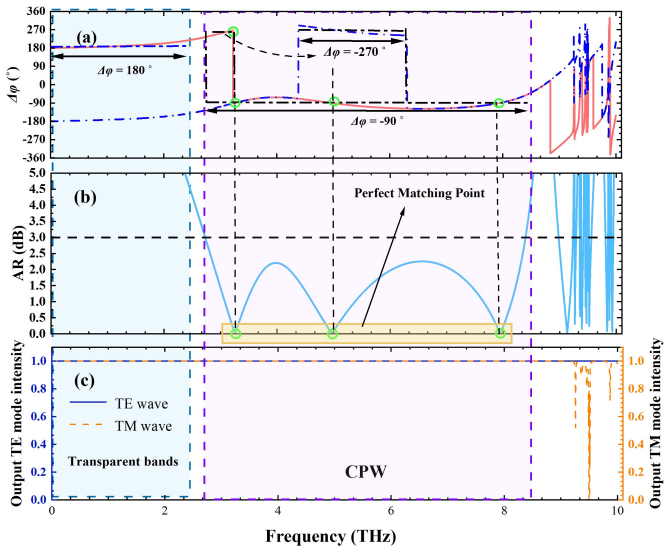

Fig.6. Output intensities and polarization characteristics of VP in 0~10 THz when the signal EW is -45° LPW (a) The variation of phase difference $\Delta\varphi$ with frequency, (b) Variation of the AR with frequency, and (c) Output characteristics of VP in the operating frequency band.

For a -45° LPW, likewise, the VP presents a broadband CTB (0~2.2 THz) and a CPPC band (2.735~8.39 THz). In both bands, the intensity of the EW emitted by the VP is hardly diminished by the simulation. In the CTB, the signal EW, with a -45° LPW, coherently interacts with the LPW that is its enantiomer. The -45° LPW propagates forward, while the +45° LPW propagates backward before emission. In CPPC bands, the -45° LPW of the signal EW acts coherently with the control EW. VP emits a forward-propagating LHCPW at port 2 while emitting a backward-propagating RHCPW at port 1. This demonstrates the ultra-wideband chiral control of the VP at -45° LPW incidence.

Similarly, in the case of a forward-propagating EW emitted from port 2. As shown in Fig.7(a), the calculation of the ellipticity χ of the PE provides us with a valuable tool to assess and quantify the effectiveness of the polarization transition.

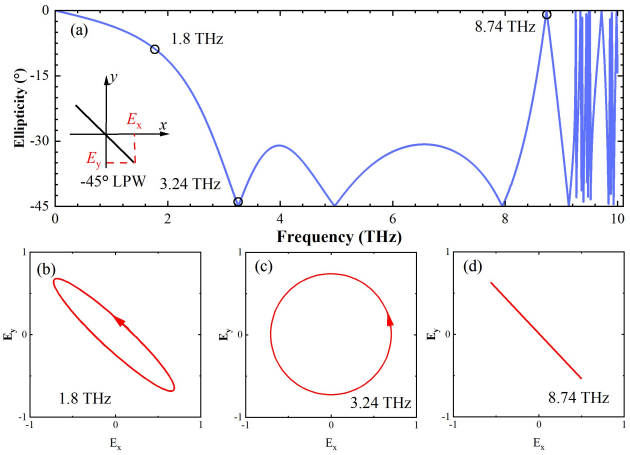

Fig.7. (a) The ellipticity χ of the PE at different operating frequencies, and the PE at three frequencies when the signal EW is -45° LPW (b) 1.8 THz, (c) 3.24 THz, and (d) 8.74 THz.

Figs.7(b)~(d) depicts the obtained PEs corresponding to frequencies of 1.8 THz, 3.24 THz, and 8.74 THz, respectively. At a frequency of 1.8 THz, the PE of a forward-propagating EW is a flat ellipse with a -45° slope. The PE of the outgoing EW is a standard circle at a frequency of 3.24 THz, which indicates that the standard LHCPW can be obtained at this perfectly matching point at this frequency of VP. It is noteworthy that the PE of the outgoing EW is a straight line at a frequency of 8.74 THz, which indicates that the polarization state of the outgoing EW is linearly polarized.

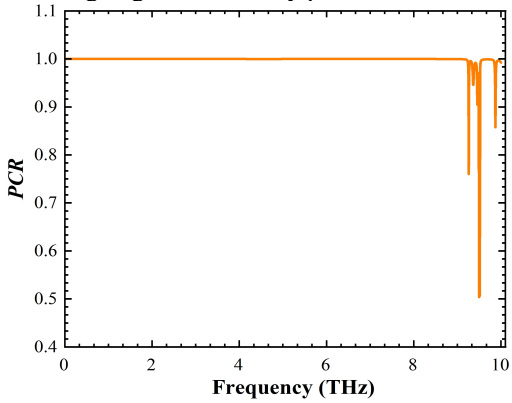

Fig.8. Trend of PCR values with different frequencies when signal EW is 45° LPW.

Authorized licensed use limited to: Nanjing Univ of Post & Telecommunications. Downloaded on April 21,2024 at 10:12:20 UTC from IEEE Xplore. Restrictions apply.
© 2024 IEEE. Personal use is permitted, but republication/redistribution requires IEEE permission. See https://www.ieee.org/publications/rights/index.html for more information.

This article has been accepted for publication in IEEE Transactions on Antennas and Propagation. This is the author's version which has not been fully edited and content may change prior to final publication. Citation information: DOI 10.1109/TAP.2024.3378388

According to the formula (15), the amount of *PCR* for VP in the case of ±45° LPW incidence is calculated, shown in Fig.8. As shown in Fig.8, the VP maintains a high *PCR* and almost maintains the original EW intensity for ejection. This reflects the very high *PCR* efficiency of the VP, which provides superior conditions for applications in antennas and other fields. The case where the incident VP is two mutually chiral CPWs will be investigated next.

When the signal EW whose polarization state is RHCPW and the control EW whose reciprocal chiral propagation direction is opposite are incident simultaneously, as shown in Fig.9, two LPWs with completely different reciprocal chiral polarization states are generated at the ports of the VP. As shown in Figs.9(a)~(b), in the CTB, two beams are generated with CPWs with different propagation directions of EWs and the same phase difference $\Delta\varphi$, while in the CPPC band, two beams of LPWs are generated with different propagation directions and the same phase difference $\Delta\varphi$. It is worth noting that, as illustrated in Fig.9(c), in terms of the value of AR, both beams generated in the CTB have an AR of less than 3 dB, and thus can be viewed as CPW, while in the CPPC band, the two beams generated have a very large AR, and thus can be considered as LPW. Fig.9(d) demonstrates the output EW intensity for the VP operating in different modes, revealing a remarkable characteristic. Within the operating frequency band, the VP showcases virtually no loss in the intensity of the EWs.

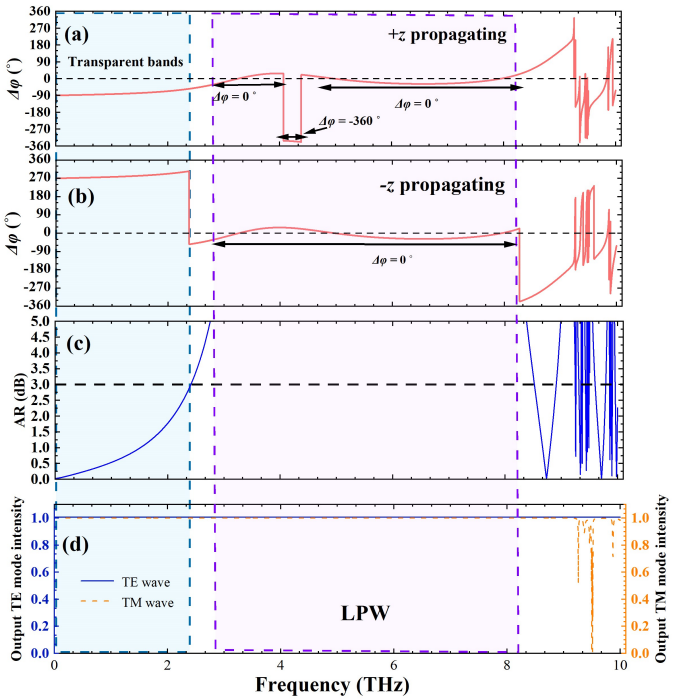

Fig.9. Output intensities and polarization characteristics of VP in 0~10 THz when the signal EW is RHCPW (a) The variation of phase difference $\Delta\varphi$ with frequency of $+z$ propagating EWs, (b) The variation of phase difference $\Delta\varphi$ with frequency of $-z$ propagating EWs, (c) Variation of the *AR* with frequency, and (d) Output properties of VP in the operating frequency band.

Similarly, the values of the ellipticity χ of the PE at RHCPW incidence for different operating frequencies are investigated, to provide a multidimensional measure. In the presence of simultaneous incidence of signal EW in LHCPW state and control EW with opposite reciprocal chiral propagation, a fascinating phenomenon occurs. Fig.10 visually demonstrates the generation of two distinct LPWs at the ports of the VP, each exhibiting a completely different reciprocal chiral polarization state. In the CTB, the VP produces the phenomenon of CPT, i.e., the two coherent EW beams pass through the VP without interfering with each other, and there is almost no change in polarization state or intensity reduction. Within the CPPC bands, as depicted in Figs.10(a)~(b) portrays the generation of two beams of LPWs, characterized by different propagation directions yet maintaining the same phase difference $\Delta\varphi$. It is important to note the distinction depicted in Fig.10(c). Within the CTB, both generated beams exhibit an AR below 3 dB, indicating their classification as CPW. However, in the CPPC band, the two beams possess a significantly larger AR, designating them as LPW. Additionally, Fig.10(d) illustrates the output EW intensity of the VP across different operational modes. Throughout the operating frequency range, the VP demonstrates negligible loss in the intensity of the EWs.

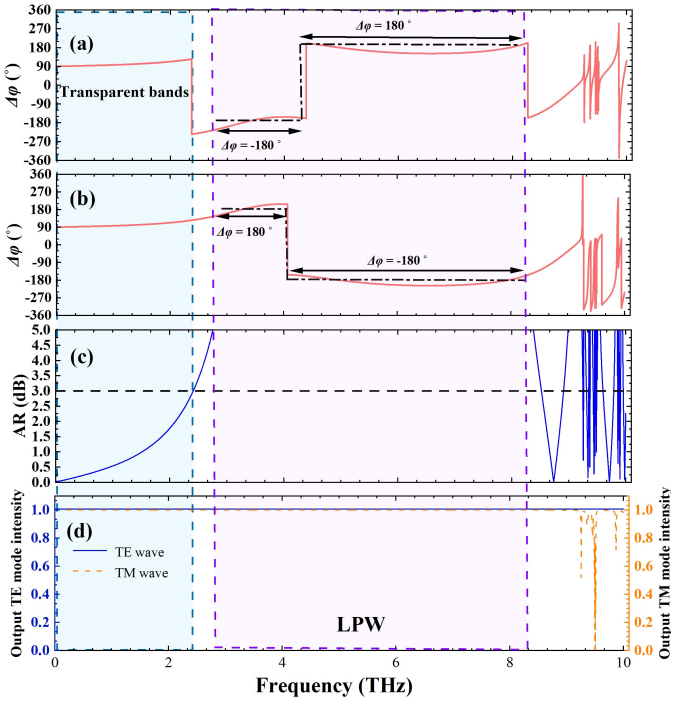

Fig.10. Output intensities and polarization characteristics of VP in 0~10 THz when the signal EW is LHCPW (a) The variation of phase difference $\Delta\varphi$ with frequency of $+z$ propagating EWs, (b) The variation of phase difference $\Delta\varphi$ with frequency of $-z$ propagating EWs, (c) Variation of the *AR* with frequency, and (d) Output properties of VP in the operating frequency band.

As shown in Fig.11(a), two beams of EWs with different orientations at the output of the two ports have their PEs of opposite ellipticity to each other, and their PEs are subsequently investigated at three special frequency points selected in Figs.11(b)~(g). Concerning $-z$ propagating EWs, their PE is symmetric about $E_x = -E_y$, while $+z$ propagating EWs, their PE is symmetric about $E_x = E_y$. The shape of the PE of the output EW at this frequency is a flattened ellipse when the frequency is 1.8 THz, the shape of the PE is exactly a straight line when the frequency is 3.24 THz, and it is

Authorized licensed use limited to: Nanjing Univ of Post & Telecommunications. Downloaded on April 21,2024 at 10:12:20 UTC from IEEE Xplore. Restrictions apply.
© 2024 IEEE. Personal use is permitted, but republication/redistribution requires IEEE permission. See https://www.ieee.org/publications/rights/index.html for more information.

This article has been accepted for publication in IEEE Transactions on Antennas and Propagation. This is the author's version which has not been fully edited and content may change prior to final publication. Citation information: DOI 10.1109/TAP.2024.3378388

noteworthy that the PE has a standard circular shape when the frequency is 8.74 THz.

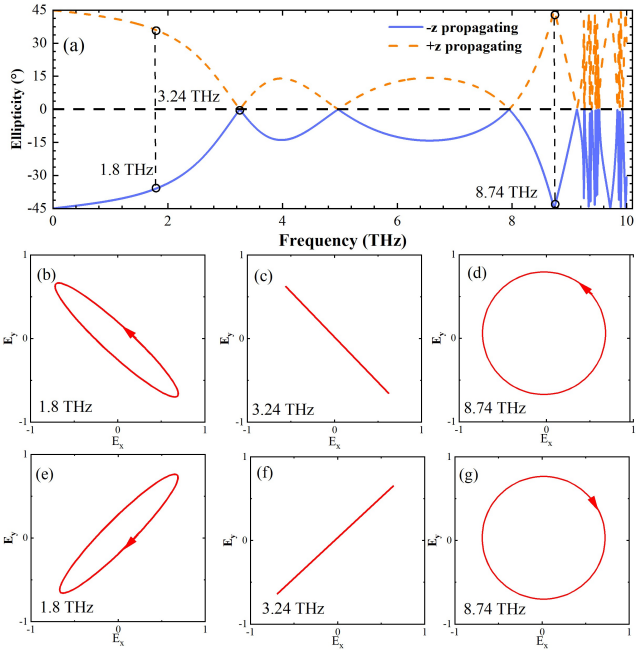

Fig.11. (a) The ellipticity χ of the PE, and the PE at three frequencies when the signal EW is -45° LPW (b) 1.8 THz (-*z* propagating), (c) 3.24 THz (-*z* propagating), (d) 8.74 THz (-*z* propagating), (e) 1.8 THz (+*z* propagating), (f) 3.24 THz (+*z* propagating), and (g) 8.74 THz (+*z* propagating).

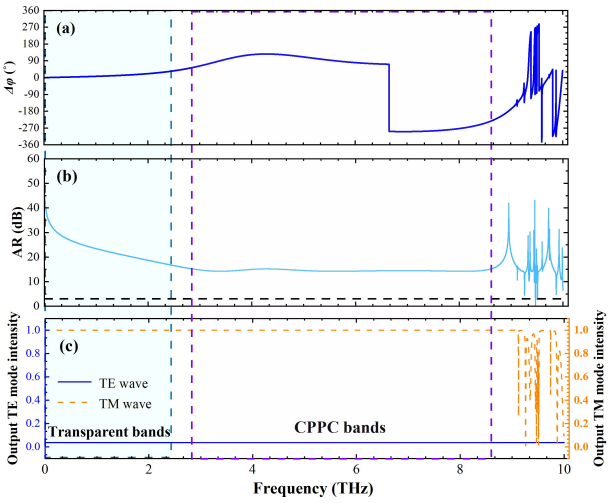

Fig.12. Output intensities and polarization characteristics of one-port incident in 0~10 THz when the signal EW is LPW (a) The variation of phase difference $\Delta\varphi$ with frequency of +*z* propagating EWs, (b) The variation of phase difference $\Delta\varphi$ with frequency of -*z* propagating EWs, (c) Variation of the *AR* with frequency, and (d) Output properties of structure in the operating frequency band.

When the EW incident from only one port, the effect of VP will disappear, which illustrates the VP's properties of coherence. As shown in Fig.12(c), EW shows selective transmission at the transmission port, with TM wave high transmission and TE wave low transmission. Meantime, there is no polarization modulation of the phase difference of EW in the two different modes, (shown in Fig.12(a)). In addition, the change in the AR from 40 dB to about 15 dB is gradually reduced and stabilized from transparent bands to CPPC bands. In this band, the VP transmits elliptically polarized waves when LPW is incident.

C. The influences of external parameters

In this section, since the angle of incidence, and the thickness and temperature characteristics of the profile are very important for the performance of physical polarizers. To prove that the VP has stability, the effects of the external parameters on the operating state of the VP are discussed. To simplify the discussion in space, only the influence of the VP by changes in the external parameters is considered here for the case where the signaling EW is incident at +45° LPW.

Fig.13 demonstrates the variation in the operating performance of the VP when the external temperature is changed. As a temperature-controllable material, InSb is extremely sensitive to temperature fluctuations, but for the stability of the VP in the operating frequency band, it is crucial to skillfully design the structure to mitigate its effect on performance.

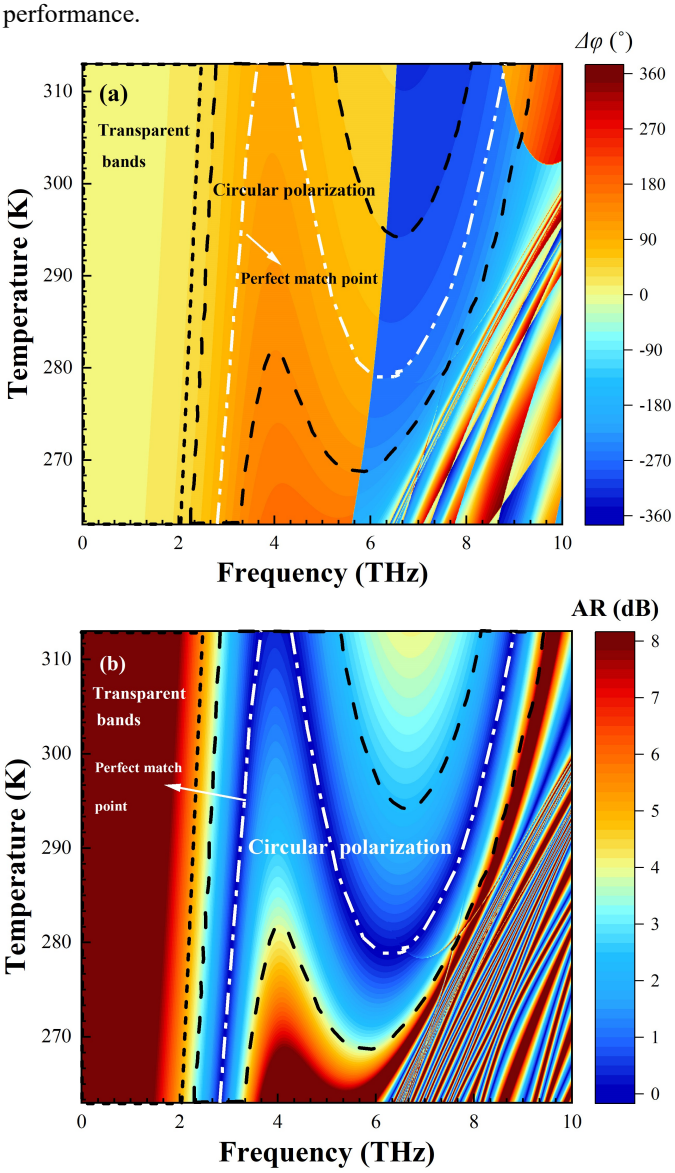

Fig.13. Effects of changes in (a) phase difference $\Delta\varphi$, and (b) *AR* with different temperatures.

Authorized licensed use limited to: Nanjing Univ of Post & Telecommunications. Downloaded on April 21,2024 at 10:12:20 UTC from IEEE Xplore. Restrictions apply.
© 2024 IEEE. Personal use is permitted, but republication/redistribution requires IEEE permission. See https://www.ieee.org/publications/rights/index.html for more information.

This article has been accepted for publication in IEEE Transactions on Antennas and Propagation. This is the author's version which has not been fully edited and content may change prior to final publication. Citation information: DOI 10.1109/TAP.2024.3378388

Herein, Fig.13 investigates the operating condition of the VP when the initial operating temperature fluctuates up and down by 50 K. According to Figs.13(a)~(b), it can be found that the CTB at low frequencies is narrowing when the temperature keeps increasing, while the CPPC band appears to be ruptured. Between these frequencies, the efficiency of the coherent PC is affected. However, the VP still maintains excellent CPPC performance in CPPC bands at temperatures between 282 K and 295 K. It is worth noting that the perfect match points are connected to a curve on which the phase difference between the TM and TE modes is constant at $90°\pm360°n$ ($n = 0, 1, 2\cdots$), with AR exactly equal to 0. In terms of phase difference $\Delta\varphi$ exhibited in Fig.13(a), the VP enables the control of the phase difference $\Delta\varphi$ in a certain temperature range and realizes ultra-wideband CPPC. From the AR shown in Fig.13(b), the CPPC, which maintains its ultra-wide bandwidth despite temperature variations, has shown excellent performance, but there is still room for improvement in high-temperature operating performance.

Fig.14 exhibits the effects of temperature dependence on the intensity of EW emitted from the VP after coherent EW enters the TE and TM modes of operation. The VP maintains excellent performance in terms of outgoing EW intensity within the operating frequency, and the loss in the process of coherent perfect control is almost negligible, which reflects the very high *PCR*.

Since the intrinsic carrier density of InSb and the surface conductivity of the graphene layer in the designed tunable structure is a function of the temperature *T*, small temperature perturbations can cause mismatches of the phase and amplitude of the chiral coherent incident EWs, and the resulting polarized standing wave is unstable. As a result, the frequency of the perfect match point varies, however, it can be figured out that the widths of the CPPC bands remain wide for a certain temperature change compared to conventional physical polarizers.

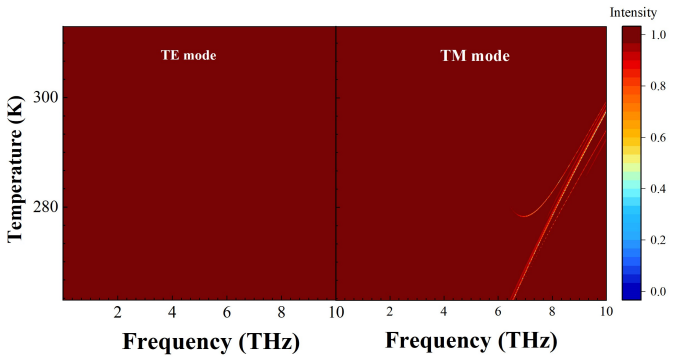

Fig.14. Effects of changes in output intensities under TE and TM mode with different temperatures.

Different incidence angles θ have a very strong influence on the electromagnetic transmission characteristics of VPs, and the stability of the wide angle is very important for the performance of VPs. Maintaining a wide-angle ultra-wideband coherent polarization control can greatly expand the application prospects of VP and increase the receptivity and temperature adaptability of VP to EWs. Here, the electromagnetic propagation properties of VP at full angle incidence are investigated, ranging from -89° to 89°.

As displayed in Figs.15(a)~(b), within a wide-angle band (-45°~45°), the VP maintains good electromagnetic transmission characteristics. Especially when the angle of incidence is ±30°, the VP maintains an ultra-broadband coherent polarization transition band, which occupies almost the entire 10 THz broadband together with the low-frequency CTB. When the angle of incidence is greater than ±45°, the CPPC band is severely damaged, while the extent of the CTB remains constant and increases slowly. At this point, the VP proves to be somewhat deficient at large angles of incidence. However, in general, the VP maintains a wide-angle ultra-wideband performance, which can meet the usage requirements.

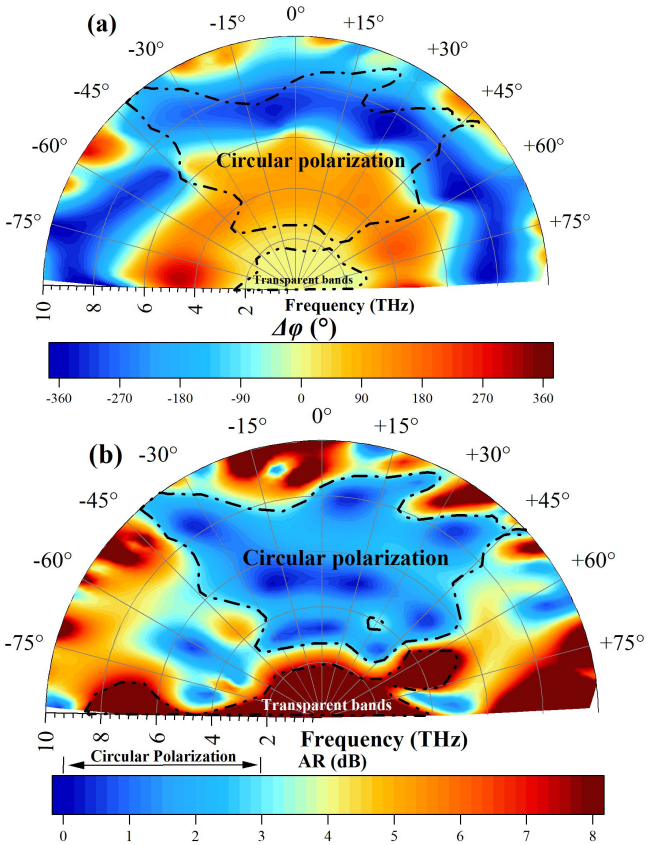

Fig.15. Effects of changes in (a) phase difference $\Delta\varphi$, and (b) *AR* with different incident angles.

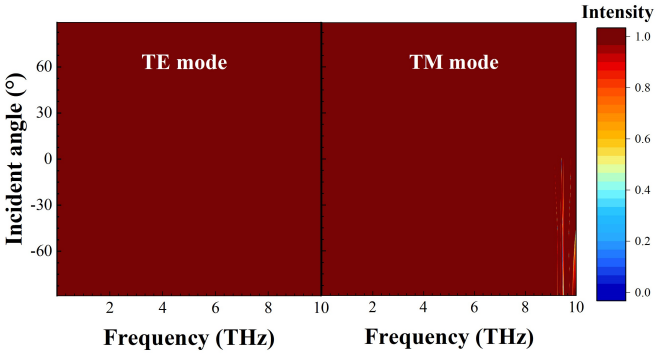

Fig.16. Effects of changes in output intensities under the TE and TM mode with different incident angles.

The incident angle dependence of the EW intensity emitted from the VP after coherent EW enters in TE and TM modes of

Authorized licensed use limited to: Nanjing Univ of Post & Telecommunications. Downloaded on April 21,2024 at 10:12:20 UTC from IEEE Xplore. Restrictions apply.
© 2024 IEEE. Personal use is permitted, but republication/redistribution requires IEEE permission. See https://www.ieee.org/publications/rights/index.html for more information.

This article has been accepted for publication in IEEE Transactions on Antennas and Propagation. This is the author's version which has not been fully edited and content may change prior to final publication. Citation information: DOI 10.1109/TAP.2024.3378388

operation is presented in Fig.16. Notably, the VP exhibits exceptional performance, maintaining a high level of outgoing EW intensity within the operating frequency range which further underscores the remarkably high *PCR* of VP.

When the incident angleθ is changed, the optical range through which the chiral coherent EWs incident on the structure is altered, which must have some effect on the phase difference, and thus affects the polarized standing waves formed, generating perturbations out of the perfectly matched points. However, simulations verified the stability of the VP at different angles, and the resulting CPPC bands were essentially unsplit.

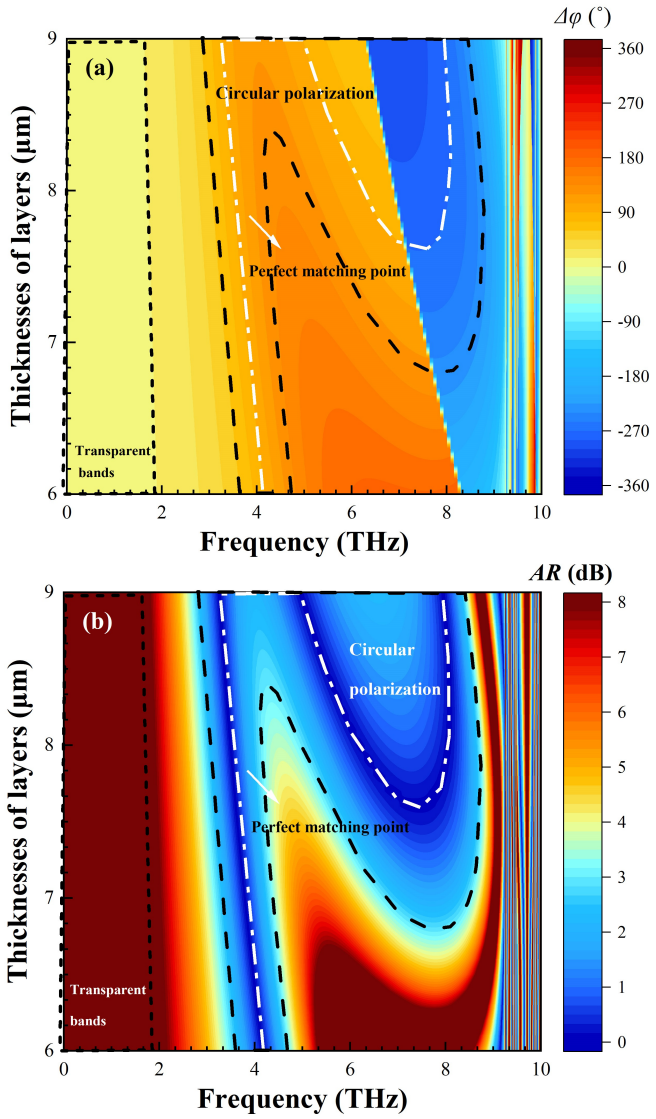

Fig.17. Effects of changes in (a) phase difference $\Delta\varphi$, and (b) *AR* with different thicknesses of dielectric layers.

In addition, the effect of the thickness of the dielectric layer on the performance of the VP is discussed, taking the dielectric TiO_2 as an example. TiO_2 thickness was set between 6~9 μm for the discussion. Likewise, by analyzing Figs.17(a)~(b), it becomes apparent that as the thickness decreases, the CTB at lower frequencies is gradually broader, while the CPPC band appears to fracture when the thickness is below 8.4 μm. This narrowing and rupture of bands significantly impact the efficiency of CPPC within these frequency ranges. However, the VP continues to exhibit exceptional CPPC performance within the CPPC bands when temperatures range from 8.4 μm to 9 μm.

Fig.18 demonstrates the incidence angle dependence of the EW intensity radiated by the VP after coherent EW enters the TE and TM modes of operation. Notably, the VP performs well, maintaining a high level of outgoing EW intensity within the functional frequency range, which indicates an extremely high *PCR* value when operating.

When the thickness of the structural dielectric is changed, the optical range through which the chiral coherent EWs travel when they are incident on the structure is altered, which must have some effect on the phase difference, which affects the frequency of the polarized standing waves that are formed, at the point of perfect matching. However, due to the stability of the standing waves formed, the bandwidth of the CPPC bands is almost unchanged within a certain thickness variation.

In the above diagrams (Figs.13, 15, and 17), a common feature can be found. As the external parameters change, the perfect match points illustrated in the figure show a linear movement. The frequency of its corresponding perfect matching point shows a bijection with the external environment variable, which represents a promising application for VP to realize external environment sensing. For space and main focus reasons, this paper focuses on the concepts, properties, and innovations that are excellent in VP-based coherent perfect chiral polarization control.

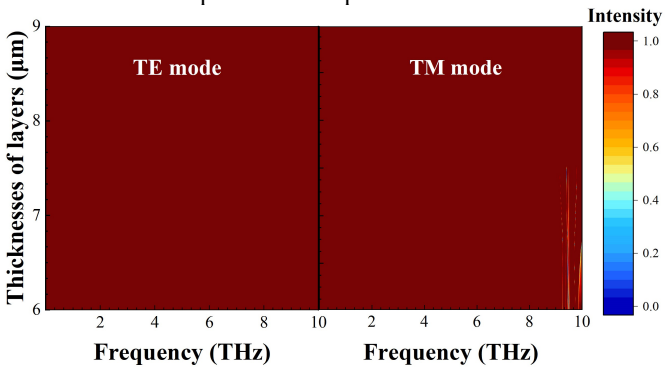

Fig.18. Effects of changes in output intensities under TE and TM mode with different thicknesses of dielectric layers.

To emphasize the distinctions between the VP and conventional physical polarizers, Table II describes the working properties of two kinds of polarizers. The ratio of the thickness of the structure to the maximum wavelength η is calculated. The polarization standing wave formed by the chiral coherent incidence EW makes the manipulation of the polarization of the VP more stable. It can be found that VP manipulation of EW has a wider operating bandwidth, *ffoc* with more conversion types relative to conventional physical polarizers. Besides, due to the transformation between energy standing waves and polarization standing waves, a transparent band is formed at low frequencies, which is not found in conventional physical polarizers. In addition, a feasible fabrication process and method for VP is provided, which can be found in Section 2 in Supplementary Material.

Authorized licensed use limited to: Nanjing Univ of Post & Telecommunications. Downloaded on April 21,2024 at 10:12:20 UTC from IEEE Xplore. Restrictions apply.
© 2024 IEEE. Personal use is permitted, but republication/redistribution requires IEEE permission. See https://www.ieee.org/publications/rights/index.html for more information.

This article has been accepted for publication in IEEE Transactions on Antennas and Propagation. This is the author's version which has not been fully edited and content may change prior to final publication. Citation information: DOI 10.1109/TAP.2024.3378388

TABLE II.
COMPARISONS FOR WORKING PROPERTIES OF CONVENTIONAL PHYSICAL POLARIZERS AND VP

	Refs.	Year	Conversion type	η	Operating bandwidth	*ffoc*	Coherent control
Conventional physical polarizers	[28]	2018	LPW to CPW	0.10	2.1~2.9 THz	32%	No
	[29]	2021	LPW to CPW	0.82	5.5~6.18 GHz	12%	No
	[30]	2021	LPW to CPW	0.1	1~2 THz	66%	No
	[31]	2023	LPW to CPW	0.91	7.5~13 GHz	53.6%	No
	[5]	2023	LPW to CPW	1.68	5.32~6.0 THz	12%	No
	[32]	2023	LPW to CPW	5.45	3.25~6.75 GHz	70%	No
VP	This work	2023	LPW to CPW CPW to LPW	2.31	2.72~8.41 THz	102%	Yes

IV. CONCLUSION

In this paper, the concept of VP is pioneered. Based on the structure of InSb and graphene layers, VP can realize the chiral polarization ultra-wideband control of coherent EW. By modulating the phase of EW in different modes, the VP is enabled to realize CTBs and CPPC bands, enabling a chiral CPPC. Meanwhile, the VP maintains an extremely high *PCR* using coherent EW control. The discussion of the effects of external environmental variables confirms that the stability of the ability of VP to control EW is strong and has a wide range of applications. Compared to the conventional physical polarizers, VP is a completely new concept, and the VP is tunable and can realization of polarization for ultra-wide bands. Meanwhile, the size of the VP is not limited by operating wavelength. This is a complete innovation in theory and of immense value as a guide to practice. The VP has a wide range of applications in antennas and propagations, logic gates, sensing, optical switching, polarization encoding, and decoding.

REFERENCES

[1] J. Hao, Y. Yuan, L. Ran, T. Jiang, J. A. Kong, C. T. Chan, L. Zhou, "Manipulating electromagnetic wave polarizations by anisotropic metamaterials." Physical review letters 99.6 (2007): 063908.

[2] A. Cerjan, S. Fan. "Achieving arbitrary control over pairs of polarization states using complex birefringent metamaterials." Physical review letters 118.25 (2017): 253902.

[3] M. Kang, Z. Zhang, T. Wu, X. Zhang, Q. Xu, A. Krasnok, ..., A. Alù, "Coherent full polarization control based on bound states in the continuum." Nature Communications 13.1 (2022): 4536.

[4] S. M. A. M. H. Abadi, N. Behdad. "Wideband linear-to-circular polarization converters based on miniaturized-element frequency selective surfaces." IEEE Transactions on Antennas and Propagation 64.2 (2015): 525-534.

[5] S. Rao, Y. Zhou, B. F. Wan, H. F Zhang. "Tunable polarization encoder capable of polarization conversion and separation based on a layered photonic structure." IEEE Journal of Selected Topics in Quantum Electronics 29.1: Nonlinear Integrated Photonics (2022): 1-8.

[6] S. Yan, G. A. Vandenbosch. "Compact circular polarizer based on chiral twisted double split-ring resonator." Applied Physics Letters 102.10 (2013).

[7] M. Mutlu, A. E. Akosman, E. Ozbay. "Broadband circular polarizer based on high-contrast gratings." Optics Letters 37.11 (2012): 2094-2096.

[8] Y. R. Wu, R. Y. Dong, J. Xu, H. F. Zhang. "A novel CPA-based layered photonic structure for multipurpose sensing applications." Optics & Laser Technology 163 (2023): 109422.

[9] D. G. Baranov, A. Krasnok, T. Shegai, A. Alù, Y. Chong, "Coherent perfect absorbers: linear control of EW with EW." Nature Reviews Materials 2.12 (2017): 1-14.

[10] S. K. Gupta, Y. Zou, X. Y. Zhu, M. H. Lu, L. J. Zhang, X. P. Liu, Y. F. Chen, "Parity-time symmetry in non-Hermitian complex optical media." Advanced Materials 32.27 (2020): 1903639.

[11] W. Wan, Y. Chong, L. Ge, H. Noh, A. D. Stone, H. Cao, "Time-reversed lasing and interferometric control of absorption." Science 331.6019 (2011): 889-892.

[12] S. A. Mousavi, E. Plum, J. Shi, N. I. Zheludev, "Coherent control of optical polarization effects in metamaterials." Scientific reports 5.1 (2015): 8977.

[13] M. Kang, Y. D. Chong, "Coherent optical control of polarization with a critical metasurface." Physical Review A 92.4 (2015): 043826.

[14] G. Pirruccio, M. Ramezani, S. R. K. Rodriguez, J. G. Rivas. "Coherent control of the optical absorption in a plasmonic lattice coupled to a luminescent layer." Physical review letters 116.10 (2016): 103002.

[15] H. Zhang, M. Kang, X. Zhang, W. Guo, C. Lv, Y. Li, ..., J. Han. "Coherent control of optical spin‐to‐orbital angular momentum conversion in metasurface." Advanced Materials 29.6 (2017): 1604252.

[16] D. G. Baranov, A. Krasnok, A. Alu. "Coherent virtual absorption based on complex zero excitation for ideal EW capturing." Optica 4.12 (2017): 1457-1461.

[17] Z. Zhang, M. Kang, X. Zhang, X. Feng, Y. Xu, X. Chen, ..., A. Alù, "Coherent perfect diffraction in metagratings." Advanced Materials 32.36 (2020): 2002341.

[18] J. Wang, W. Wu, Cavity-based linear-to-circular polarization converter." Optics Express 25.4 (2017): 3805-3810.

[19] L. Young, L. A. Robinson, C. A. Hacking, "Meander-line polarizer." IEEE Transactions on Antennas and Propagation 21.3 (1973): 376-378.

[20] M. Huang. "Stress effects on the performance of optical waveguides." International Journal of Solids and Structures 40.7 (2003): 1615-1632.

[21] H. H. Li, "Refractive index of alkaline earth halides and its wavelength and temperature derivatives." Journal of physical and chemical reference data 9.1 (1980): 161-290.

[22] L. M. Qi, Z. Q. Yang, F. Lan, X. Gao, and Z. J. Shi, "Properties of obliquely incident electromagnetic wave in one-dimensional magnetized plasma photonic crystals." Physics of Plasmas 17.4 (2010).

[23] J. Sui, S. Liao, R. Dong, H. F. Zhang, "A Janus Logic Gate with Sensing Function." Annalen der Physik 535.4 (2023): 2200661.

[24] A. Andryieuski, and A. V. Lavrinenko. "Graphene metamaterials based tunable terahertz absorber: effective surface conductivity approach." Optics express 21.7 (2013): 9144-9155.

[25] B. Lin, J. L. Wu, X. Y. Da, W. Li, J. J. Ma. "A linear-to-circular polarization converter based on a second-order band-pass frequency selective surface." Applied Physics A 123 (2017): 1-5.

[26] W. H. McMaster. "Polarization and the Stokes parameters." American Journal of Physics 22.6 (1954): 351-362.

Authorized licensed use limited to: Nanjing Univ of Post & Telecommunications. Downloaded on April 21,2024 at 10:12:20 UTC from IEEE Xplore. Restrictions apply.
© 2024 IEEE. Personal use is permitted, but republication/redistribution requires IEEE permission. See https://www.ieee.org/publications/rights/index.html for more information.

This article has been accepted for publication in IEEE Transactions on Antennas and Propagation. This is the author's version which has not been fully edited and content may change prior to final publication. Citation information: DOI 10.1109/TAP.2024.3378388

[27] J. Zhang, C. Guo, K. Liu, Z. Zhu, W. Ye, X. Yuan, S. Qin. "Coherent perfect absorption and transparency in a nanostructured graphene film." Optics express 22.10 (2014): 12524-12532.
[28] L. Peng, X. F. Li, X. Jiang, S. M. Li "A novel THz half-wave polarization converter for cross-polarization conversions of both linear and circular polarizations and polarization conversion ratio regulating by graphene." Journal of Lightwave Technology 36.19 (2018): 4250-4258.
[29] S. Y Wang, J. D Bi, W. Liu, W. Geyi, S. Gao "Polarization-insensitive cross-polarization converter." IEEE Transactions on Antennas and Propagation 69.8 (2021): 4670-4680.
[30] M. Amin, O. Siddiqui, H. Abutarboush, M. Farhat, R. Ramzan. "A THz graphene metasurface for polarization selective virus sensing." Carbon 176 (2021): 580-591.
[31] M. Magarotto, L. Schenato, P. De. Carlo, A. D. Capobianco "Plasma-based reflective surface for polarization conversion." IEEE Transactions on Antennas and Propagation 71.3 (2023): 2849-2854.
[32] W. Zhang, B. Li, and L. Zhu. "Orthogonal adjacent-order filtering element-based wideband transmissive linear-to-circular polarization converter." IEEE Transactions on Antennas and Propagation 71.4 (2023): 3324-3334.

You-Ran Wu was born in Jiangsu, China, in 2002. He is currently learning in Nanjing University of Posts and Telecommunications, Nanjing, China. His main research interests involve photonic crystals and coherent perfect absorption.

Rui-Yang Dong was born in Jiangsu, China, in 2002. He is currently learning in Nanjing University of Posts and Telecommunications, Nanjing, China. His main research work is the photonic time crystal.

Hai-Feng Zhang was born in Jiangxi, China, in 1978. He received the M.Sc. degree in electronics science and technology from Nanchang University, Nanchang, China, in 2008. In 2014, He received the Ph.D. degree in College of Electronic and Information Engineering, Nanjing University of Aeronautics and Astronautics, Nanjing, China. He is currently working as a professor at College of Electronic and Optical Engineering & College of Flexible Electronics (Future Technology), Nanjing University of Posts and Telecommunications, Nanjing, China. His main research interests include the computational electromagnetics, plasma photonic crystal, plasma stealthy and electromagnetic properties of metamaterials.

Authorized licensed use limited to: Nanjing Univ of Post & Telecommunications. Downloaded on April 21,2024 at 10:12:20 UTC from IEEE Xplore. Restrictions apply.
© 2024 IEEE. Personal use is permitted, but republication/redistribution requires IEEE permission. See https://www.ieee.org/publications/rights/index.html for more information.